

# Corrosion Behaviour of Aluminium Matrix Composite Reinforced with Boron Carbide in 3.5% NaCl

Zaifol Samsu<sup>1,3</sup>, Norinsan Kamil Othman<sup>1,\*</sup>, Mohd Suzeren Md Jamil<sup>2</sup>, Hafizal Yazid<sup>3</sup>  
and Mohd Sofian Alias<sup>1</sup>

<sup>1</sup>Material Science Program, Department of Applied Physics, Faculty of Science and Technology,  
Universiti Kebangsaan Malaysia, 43600 Bangi, Selangor, Malaysia

<sup>2</sup>Department of Science Chemistry, Faculty of Science and Technology, Universiti Kebangsaan Malaysia,  
43600 Bangi, Selangor, Malaysia

<sup>3</sup>Material Technology Group, Industrial Technology Division, Malaysian Nuclear Agency, Bangi,  
43000 Kajang, Selangor, Malaysia

## ABSTRACT

*The corrosion behavior of Aluminium matrix composite reinforced with micro-size boron carbide was investigated in a 3.5% NaCl solution. The sample was prepared using the stir casting technique with compositions of 2, 4, 6, 8 and 10 wt% of B<sub>4</sub>C particles. Potentiodynamic polarisation methods were used to derive the electrochemical parameters while hardness analysis methods were used to derive the mechanical properties. A field emission scanning electron microscope (SEM) was employed to investigate the particle boron carbide distribution on the matrix and surface morphology of the metal surface before and after the corrosion test. The X-ray diffraction (XRD) analysis was used to investigate the received powders and matrix samples for phase recognition and the presence of reinforcement particles (B<sub>4</sub>C) in the composite samples. The findings demonstrated that in a 3.5% NaCl solution, the aluminium matrix composite corrosion rate was inferior to that of the base alloy. At the same time, the corrosion rates of the composite increased with the increase in the composition of B<sub>4</sub>C in matrix aluminium. Passive layer breakdown due to agglomeration of boron carbide particles caused the increased corrosion rate. Hardness analysis has shown that the value of hardness was improved with the increase in the composition of B<sub>4</sub>C in the aluminium matrix.*

**Keywords:** Aluminium matrix composite, Boron Carbide, Corrosion, 3.5% NaCl, Hardness

## 1. INTRODUCTION

The aerospace and automotive industries have encountered significant technological hurdles while striving to meet the demands and expectations of consumers. A predominant preference among manufacturers and designers is evident for materials that offer weight reduction advantages to meet their diverse needs. In the context of aircraft, a reduction in weight holds the potential to yield significant advantages, including decreased fuel consumption, augmented payload capacity [1] heightened performance, and a consequential reduction in emissions [2]. The overarching priorities in both the aircraft and automotive industries, particularly with the emergence of electric vehicles, are centered around cost reduction and weight minimization. Consequently, there arises an imperative need to explore advanced materials that align with these objectives [3, 4]. In the pursuit of developing cutting-edge materials tailored to meet the requirements of discerning clients, researchers have dedicated their efforts to the field of composite materials over recent decades.

\* Corresponding authors: insan@ukm.edu.my

As a result of its use in electric vehicles (EVs), solar panels, wind turbines, gearbox lines for power, and other products, aluminium demand is expected to increase. The European Aluminium Association predicts that by 2030, the annual demand from the EV sector will amount to 12 million tonnes of aluminium, with manufacturers needing 250 kg of aluminium for every EV [5].

According to experts, using aluminium instead of steel improves durability, performance, safety, fuel efficiency, and many other environmental factors. Any electric vehicle (EV) can enhance its range by an additional 10-15% for every 100 kg saved. In addition, more range is essential to promote EV adoption and close the gap with Internal combustion engine vehicles.

The materials used to build automobiles and aeroplanes should be lightweight, have a high specific strength, be able to withstand high temperatures, fatigue loads, corrosion, and cracking, and have a low wear rate. In the past, alloy steels were typically employed for parts of aeroplanes and automobiles. The advantages of ferrous metals are their widespread availability and low cost, but their disadvantages include their heavy weight, increased wear rate, and lower corrosion resistance. Aluminium, magnesium, titanium, and other nonferrous metals have garnered considerable interest for use in a variety of applications due to their lower densities than ferrous metals. Magnesium (Mg) is one of the nonferrous elements that is lightweight, but its usage in aircraft and automotive manufacture is limited because it seizes fire [6, 7]. Aluminium (Al) costs 20 to 30 times less than titanium (Ti), which expends an amount of weight similar to magnesium (Mg). Since aluminium alloy (AA) is more durable than the majority of magnesium alloys, it is frequently utilized [8].

In comparison to monolithic materials, aluminium matrix composites (AMCs) offer a greater mix of mechanical, physical and thermal qualities. There are three type of common reinforcement that been used like alumina ( $\text{Al}_2\text{O}_3$ ), silicon carbide (SiC) and boron carbide ( $\text{B}_4\text{C}$ ). Boron carbide have an advantage compare with SiC and  $\text{Al}_2\text{O}_3$ , specifically density ( $2.51 \text{ g.cm}^{-3}$ ) [9] which is much less than  $\text{Al}_2\text{O}_3$  and SiC, a very high degree of hardness ( $H_v = 30\text{GPa}$ ) and wear resistance, a surprising lack of chemical activity [10] and unique capability neutron absorption [11]. These characteristics make  $\text{B}_4\text{C}$  a great reinforcement for high performance of metal matrix composite.

The impact of the reinforcing particles on the corrosion resistance is one of the primary difficulties when employing Al-based metal matrix composite. Due to the fact that the continuousness of the aluminium matrix and its protective surface oxide layers is disrupted by the addition of reinforcement particles, there are more potential sites for corrosion to start, making the aluminium composite more prone to corrosion [12]. The researcher has been investigate the effect of SiC particle in aluminium composite on the corrosion behavior of 2014 Al-Cu alloy in the 3.5% NaCl [13]. They discovered that adding 25 wt% SiC particles to the aluminium alloy significantly reduces corrosion resistance. Another researcher employed the potentiodynamic polarization technique to examine the corrosion characteristics of the 6061 Al-Si particle composite and its corresponding aluminum-based alloy [14]. Their investigation revealed that the aluminum matrix composite exhibited an accelerated corrosion rate compared to the aluminum base alloy, with the primary locus of corrosion occurring at the interface, as opposed to the uniform corrosion observed in the case of the aluminum base alloy

In the present context, there is a noticeable paucity of research findings dedicated to the corrosion aspects of Al- $\text{B}_4\text{C}$  composites, especially when juxtaposed with the abundant research endeavors directed towards comprehending the corrosion characteristics of Al-SiC composites. This study delves into the evaluation and scrutiny of the influence of varying proportions of reinforcing  $\text{B}_4\text{C}$  particles within the aluminum alloy AA6061, specifically focusing on the formation of a passive film in a seawater environment [15]. According to their findings, the corrosion potential of  $\text{B}_4\text{C}$  particle reinforced AA6061 alloy shifted in favour of the positive direction when assessed to the base alloy, which led to the development of a passive layer.

In this investigation, Al6061/B<sub>4</sub>C composite was fabricated with different percentage of weight fraction of B<sub>4</sub>C using stir casting technique. The investigation was conducted in ambient air to gain a thorough realizing of the corrosion behaviors and corrosion mechanism of AA6061-B<sub>4</sub>C matrix composites in a 3.5 wt% NaCl solution. Electrochemical technique and hardness analysis were used. A Field Emission Scanning Electron Microscope (FESEM) was employed to assess the surface morphology and material surface structure of the composite, both before and after exposure to corrosion. Furthermore, an investigation was conducted to elucidate how alterations in the weight percentage of B<sub>4</sub>C particles affect the corrosion behavior and hardness properties of Al-B<sub>4</sub>C composites. The analysis aimed to discern prevailing trends and pinpoint the optimal composition for enhanced corrosion resistance, taking into account the fluctuating weight percentage of B<sub>4</sub>C particles.

## 2. MATERIAL AND METHODS

### 2.1 Chemical Composition of Material

AL6061 finds widespread application in the aircraft and automotive sectors due to its exceptional resistance to corrosion and notable strength relative to other aluminum alloys. This material is readily available from local suppliers in the commercial market. Table 1 provides a comprehensive breakdown of the elemental constitution of the base alloy, as determined through the utilization of Spark Emission spectroscopy (SES) (Model WAS Foundry-Master, Oxford Instruments)

**Table 1** Chemical composition of Al 6061 base alloy

Element	Si	Fe	Cu	Mn	Mg	Cr	Al
Composition (wt.%)	0.5	0.41	0.21	0.12	0.76	0.21	Balance

### 2.2 Reinforcement Material

Boron carbide (B<sub>4</sub>C), with an impressive purity level of 99.95%, was selected as the primary reinforcing material for this investigation due to its exceptional attributes. These attributes include remarkable resistance to corrosion and wear, coupled with enhanced mechanical properties encompassing tensile strength, hardness, and impact resistance. In preparation for the casting process, the boron carbide particles underwent a meticulous preheating procedure at 300°C, a step undertaken to eliminate gases and prevent any unwanted temperature fluctuations. The boron carbide reinforcement particles, supplied from Yemate Ind China, exhibited an average particle size of 15µm.

### 2.3 Stir Casting

Aluminum alloy 6061-based composite materials, incorporating reinforcement from boron carbide, were fabricated using a two-stage stir casting procedure. Overcoming challenges related to wetting effects and chemical interactions between the reinforcements and the matrix posed significant obstacles when employing the stir casting technique for composite production [16]. Addressing this challenge is imperative for achieving the desired composite properties and ensuring the overall success of the composite manufacturing process.

Initially, aluminum foil served as a containment medium for boron carbide, fulfilling a dual role of facilitating its uniform dispersion within the molten metal matrix and preventing its migration towards the slag phase [17]. Aluminum 6061 was brought to a liquid state using a precision digital electric melting furnace with a capacity of up to 1 kg of gold (Brand Jerlus). This custom-designed

apparatus was exclusively tailored for the casting process. The molten composite underwent stirring via a stainless-steel impeller, with a temperature control system regulating the heating and cooling rates.

A furnace, boasting a melting point of 700°C, was employed to liquefy a substantial quantity of aluminum. Upon complete melting of the aluminum, the resultant slurry underwent a carefully controlled cooling process, gradually reducing its temperature below the liquidus threshold, thereby maintaining it in a semi-solid state. The reinforcement particles, comprising varying compositions of 2, 4, 6, 8, and 10 wt% B<sub>4</sub>C, respectively, were enclosed in aluminum foil and introduced into the molten metal.

In pursuit of moisture elimination and easily mingle with the molten metal, the foiled boron carbide was initially preheated independently at the temperature of 300°C. Subsequently, the mixture of boron carbide and aluminum was reheated to 700°C and continuously stirred at 100 rpm for a duration of 30 minutes. Subsequently, the molten metal resulting from the stir-casting process was carefully poured into the mold and permitted to undergo controlled solidification. The resulting samples were then carefully sectioned and subjected to detailed analysis.

## 2.4 Metallographic Examination

The test specimens underwent a mechanical grinding process using abrasive papers spanning from 120 grit to 640 grit. Subsequently, they were subjected to a polishing procedure employing diamond paste with particle sizes of 3 μm and 1 μm, respectively. These preparations were carried out following the precision cutting of the specimens into dimensions measuring 30 mm x 20 mm x 5 mm. Keller's reagent solution with etching for 10 seconds was used to analyze the microstructure after deep etching to reveal the interfacial microstructure between aluminium base alloy matrix and B<sub>4</sub>C and then followed by cleaning with acetone.

Microscopic images of the sample surfaces were acquired by employing a Field Emission Scanning Electron Microscope (FESEM Model Zeiss GeminiSEM 500). These images were used to analyze B<sub>4</sub>C particles distribution, percentage area as well as interfaces between B<sub>4</sub>C and Al6061. The identification of B<sub>4</sub>C particle presence and the evaluation of contact properties were accomplished through the utilization of Oxford Instrument's Energy Dispersive X-ray Analysis (EDX) with the X-Max 80 model, as well as X-ray Diffraction (XRD) analysis conducted with the X'Pert Pro model from Brand Panalytical.

## 2.5 Electrochemical Study

An electrochemical workstation was used to conduct electrochemical measurements with the model of Reference 600 instruments (Gamry Instruments, Warminster, PA, USA). The electrochemical performance was accomplished using a three-electrode compartment cell. The working electrode was fabricated aluminium composite or base alloy for analysis. As the reference and counter electrodes, respectively, a silver/silver chloride electrode (Ag/AgCl) and a graphite electrode were utilized. Electrode potentials were assessed with respect to silver/silver chloride electrode (Ag/AgCl). The polarization experiment was done immediately after one hour corrosion potential running on the similar electrode with no additional surface treatment. The experiments were conducted under ambient temperature.

### 2.5.1 Tafel Polarization

A corrosion environment with comprising a 3.5% sodium chloride solution was utilized to expose finely polished specimens of both the composite and the base alloy. This exposure aimed to ascertain the establishment of a stable open circuit potential (OCP). The specimen was polarised to -250 mV cathodically and +250 mV anodically with respect to the OCP at a scan rate of 1 mV/s to record the potentiodynamic current-potential curves.

## 3. RESULTS AND DISCUSSION

### 3.1 Microstructural Characterization

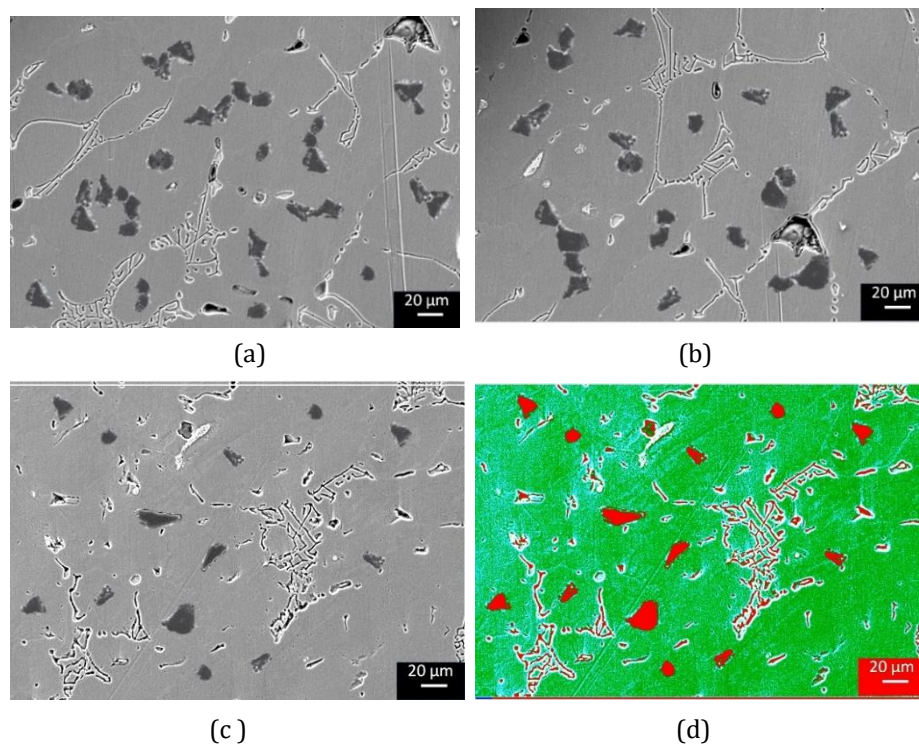


**Figure 1.** SEM micrographs showing etched surface of stir casting aluminium alloy (6061) matrix composite with (a) 2, (b) 6, (c) 10 wt% B<sub>4</sub>C and (d) image analysis of Al-2%B<sub>4</sub>C.

Figure 1 presents microstructural imagery obtained via Field Emission-Scanning Electron Microscopy (FESEM). These images portray the intricate composition of Al 6061 matrix composites, featuring varying weight percentages of 2%, 6%, and 10% B<sub>4</sub>C. These composites were meticulously crafted using a sophisticated two-step stir casting procedure. In these micrographs, the darker regions correspond to the presence of boron carbide. Achieving a homogeneous distribution of boron carbide within the aluminum matrix is pivotal in the production of aluminum matrix composites. As evident in Figure 1(a), it is evident that the second-phase reinforcement is uniformly dispersed throughout the matrix, devoid of any clustering or segregation. However, an increase in the weight fraction of boron carbide results in the agglomeration of reinforcement particles within the aluminum matrix. Notably, an elevation in the volume fraction of reinforcement leads to increased porosity and clustering [18]. It is noteworthy that the utilization of a two-step stir casting technique facilitates the uniform dispersion of a high-volume fraction of B<sub>4</sub>C particles within the aluminum matrix. Furthermore, it has been revealed that the incorporation of magnesium into the AA6061 alloy enhances the interaction between particles, effectively reducing the surface tension of the molten alloy [19].

### 3.2 XRD Analysis

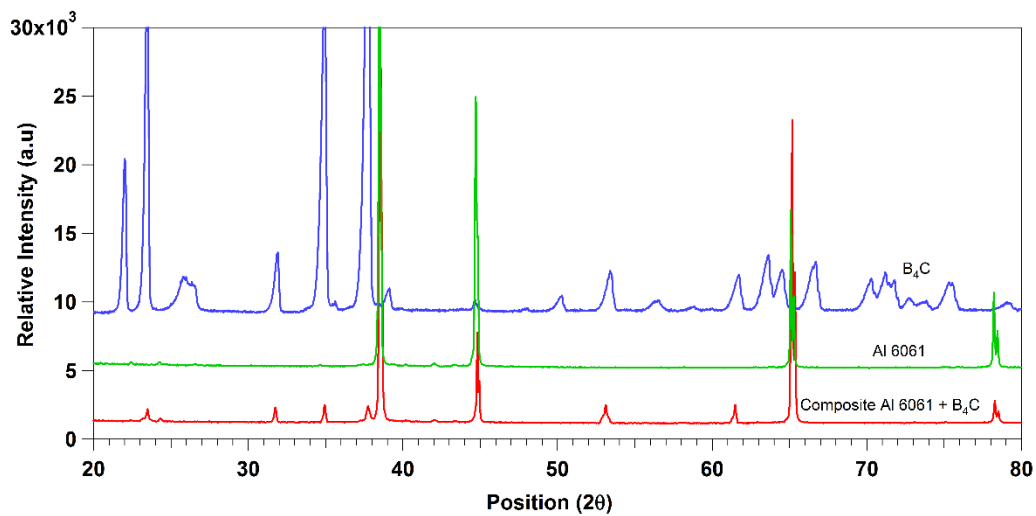


**Figure 2.** XRD analysis of B<sub>4</sub>C particle, Al6061 and Al-10%B<sub>4</sub>C composite.

X-ray Diffraction (XRD) investigations were conducted on Al6061-based composites to validate the presence of B<sub>4</sub>C as a reinforcing constituent and to discern any potential additional phases. These composites were composed of 10wt% B<sub>4</sub>C particles incorporated within an aluminum matrix of 6061, as visually represented in Figure 2. The lower section of Figure 2 displays the X-ray diffraction pattern and findings for the Al 6061 alloy containing 10 wt% B<sub>4</sub>C in the aluminum matrix composite. In the X-ray diffraction pattern, a total of seven peaks were observed within the 2θ range spanning from 20 to 80. Specifically, the peaks at 2θ values of 23.50°, 34.92°, and 37.69° correspond to B<sub>4</sub>C, while those at 2θ values of 38.51°, 44.82°, 65.18°, and 78.28° are attributed to pure aluminum. The remaining minor peaks are ascribed to impurities.

### 3.3 Corrosion Rate Analysis of Al-B<sub>4</sub>C Composites using TAFEL

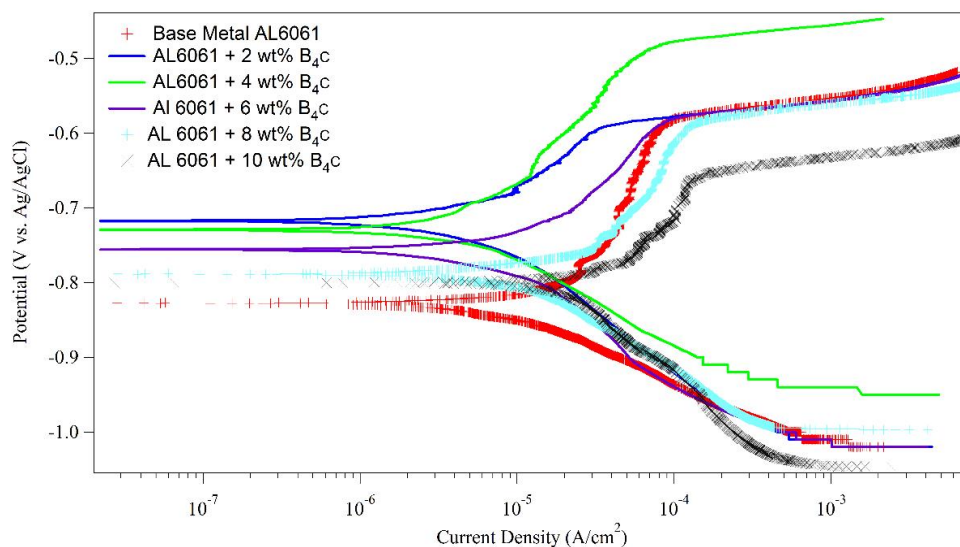


**Figure 3.** Tafel plot polarization curves of aluminium 6061 and its B<sub>4</sub>C composite in 3.5% NaCl. (Potential scanning rate 1mV/s at 25°C ±2.

**Table 2** Electrochemical characteristics calculated from the polarization behaviour of the Al-B<sub>4</sub>C composites in 3.5% NaCl

B <sub>4</sub> C content (wt%)	E <sub>corr</sub> (mV vs Ag/AgCl)	I <sub>corr</sub> (μA/cm <sup>2</sup> )	β <sub>c</sub> (mV/dec)	β <sub>a</sub> (mV/dec)	Corrosion rate (μm/yr)
0	-827.6	5.684	130.8	316	62.57
2	-717.2	1.716	154.9	137.4	18.89
4	-732.6	1.879	121.7	228.4	20.69
6	-755.7	3.011	170.4	159.7	33.15
8	-788.4	7.394	188.3	235.2	81.39
10	-800.6	11.11	235.4	179.7	122.3

The impact of aluminum composites reinforced with varying compositions of B<sub>4</sub>C particles on polarization behavior was investigated under ambient temperature conditions. The results were captured in Tafel plots, and key kinetic parameters were extracted and summarized in Table 2, as well as visually depicted in Figure 3. Table 2 provides an overview of the corrosion potential, corrosion current density, and anodic-cathodic Tafel slope. These parameters are vital indicators of a material's corrosion behavior.

The data reveals a notable increase in the corrosion current density (I<sub>corr</sub>) from 1.716 to 11.11 μA/cm<sup>2</sup> as the boron carbide composition rises from 2% to 10 wt.%. This signifies a significant escalation in the corrosion rate of the composite with an increasing content of boron carbide. It's worth noting that a slight increase in the boron carbide content (less than 6 wt.%) leads to a lower corrosion rate compared to the base alloy. However, when the boron carbide content exceeds 8 wt.%, the corrosion rate surpasses that of the base alloy. Analysis of the data reveals that the aluminum composite containing 2 wt.% B<sub>4</sub>C exhibits the lowest corrosion current (I<sub>corr</sub>) in comparison to the base alloy. Conversely, the addition of 8 and 10 wt.% B<sub>4</sub>C significantly elevates the corrosion rate of the composite. This heightened corrosion rate can be attributed to the substantial irregular distribution of B<sub>4</sub>C particles, resulting in their agglomeration within the aluminum matrix and subsequent breakdown of the passive aluminum oxide layer. The agglomeration of B<sub>4</sub>C introduces discontinuities in the passive layer, creating pathways for aggressive ions to penetrate, thus accelerating corrosion.

The corrosion potential exhibited a noticeable shift in the positive direction, transitioning from -827.6 mV to -717.2 mV when 2 wt% of B<sub>4</sub>C was introduced into the composite. However, this trend did not persist as the content of B<sub>4</sub>C increased up to 10 wt%. This deviation from the anticipated behavior aligns with the mixed potential hypothesis, which postulates that an increase in the B<sub>4</sub>C content within the composite should result in a shift towards a more noble potential [15]. Contrary to this expectation, the introduction of higher levels of B<sub>4</sub>C into the composite led to a reversal of this shift, causing the potential to move in a negative direction. This unexpected reversal can be attributed to the fact that as the B<sub>4</sub>C content increases, the continuity of the protective surface oxide layers diminishes. This renders the Al-10 wt.% B<sub>4</sub>C composite more susceptible to the presence of chloride ions, consequently resulting in a less noble electrochemical potential.

In summary, the study reveals a complex relationship between the content of B<sub>4</sub>C reinforcement and the corrosion behavior of the aluminum composites. While low concentrations of B<sub>4</sub>C can enhance corrosion resistance, excessive amounts lead to agglomeration, passive layer breakdown, and heightened corrosion rates. These findings emphasize the critical role of particle distribution and dispersion in determining the corrosion performance of composite materials.

### 3.4 Pit Morphology after Tafel Polarization

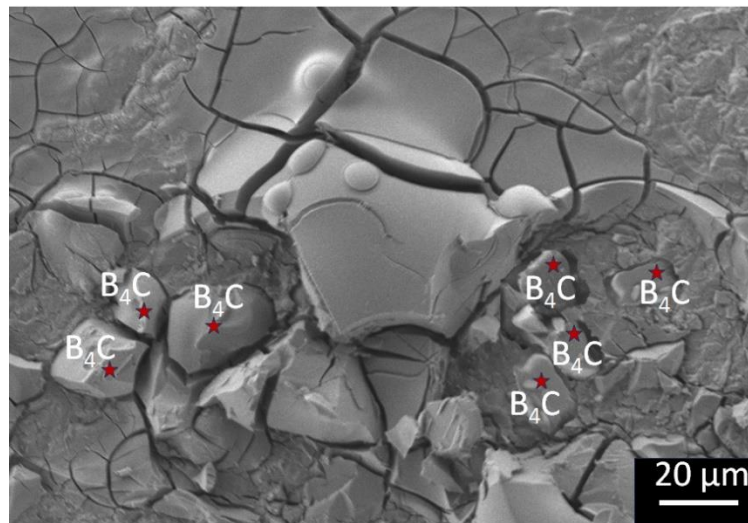


**Figure 4.** FESEM image showing the occurrence of pitting and surface cracking at the interface of aluminium matrix and  $B_4C$  particles on an AA6061-10 wt%  $B_4C$  surface during polarization in a 3.5% NaCl solution.

Figure 4 provides a visual depiction of the surface morphology post-corrosion, revealing evident film breakage in the vicinity of the  $B_4C$  particles. Notably, the scanning electron microscope (SEM) image showcases pit initiation at the interface of Al and  $B_4C$ . These pits exhibit varying characteristics, with those near the  $B_4C$  particles being notably deeper than the others.

The formation of these pits is attributed to the agglomeration of  $B_4C$  particles, leading to an increased surface area ratio between the particles and the aluminum matrix. This heightened surface area ratio enhances the likelihood of pit initiation. The underlying mechanism involves  $B_4C$  particles disrupting the continuity of adjacent aluminum oxide layers, thereby creating discontinuities that facilitate the ingress of aggressive chloride ions into the matrix. Upon contact with the matrix, these chloride ions induce pitting corrosion [20]. Furthermore, it's important to note that the cathodic relationship between  $B_4C$  particles and the Al matrix, along with the generation of hydroxyl groups, elevates the pH around the  $B_4C$ -Al matrix interphase. This, in turn, results in the dissolution of aluminum and the formation of circular pits around the  $B_4C$  inclusions.

In summation, the microphotography analysis conducted after polarization tests underscores the substantial influence of the weight fraction of ceramic particles ( $B_4C$ ) in expediting the corrosion process. The formation of pits and the disruption of protective oxide layers, driven by the agglomeration of  $B_4C$  particles, play a pivotal role in the corrosion behavior observed in the composite.

### 3.5 Hardness Analysis

The mechanical characteristics of the AA6061 matrix alloy demonstrated improvement with an increase in the weight fraction of  $B_4C$ . In Figure 5, a correlation between the weight fraction (%wt.) of  $B_4C$  reinforcement particles and the hardness value of the fabricated aluminum matrix composite is illustrated. Notably, a linear relationship is observed, wherein the macrohardness of the aluminum matrix composite steadily rises with an elevation in the proportion of reinforcement particulates. This augmentation in the reinforcement particle content within the matrix leads to an expansion of the surface area of the reinforcement material, consequently resulting in a reduction of the matrix grain sizes.



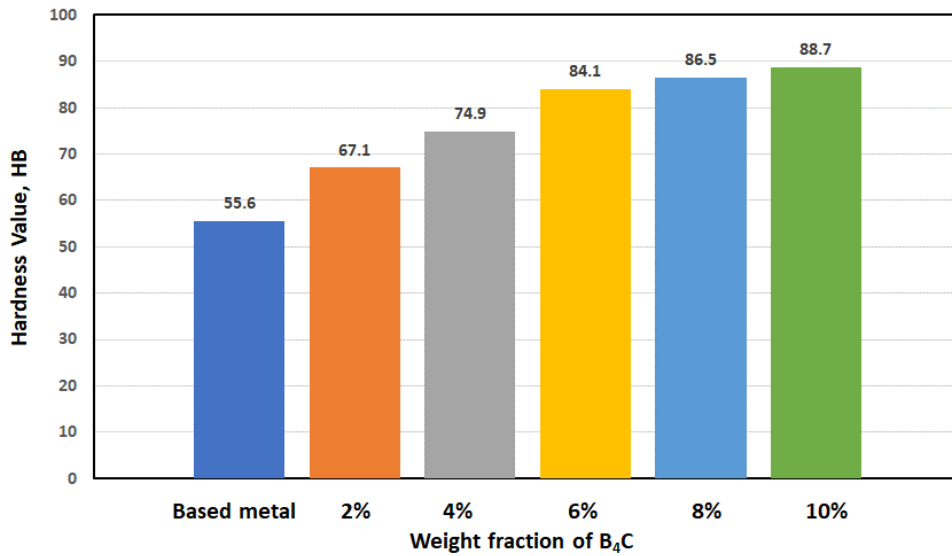


**Figure 5.** Bar chart of micron size B<sub>4</sub>C particle wt% with brinell hardness.

The presence of a robust surface layer on these particles imparts greater resistance to plastic deformation, thereby leading to an enhancement in the composite's hardness. As noted in a previous study [21] the introduction of hard ceramics into a soft, ductile matrix results in a substantial increase in hardness values at the cost of ductility. Consequently, the incorporation of hard reinforcement particles elevates the ability of the metal matrix composite to bear loads, constrains matrix deformation by limiting disruptive displacements, and ultimately augments the overall strength of the composites[22]. These findings align harmoniously with the outcomes presented by Kalaiselvan [23] and are consistent with the insights offered in the review article authored by Sambathkumar [24]

#### 4. CONCLUSION

In summary, the findings underscore the effectiveness of the two-step stir casting technique in achieving a uniform dispersion of boron carbide within the aluminum matrix. Nevertheless, augmenting the weight fraction of boron carbide resulted in the aggregation of reinforcement particles within the aluminum matrix. This agglomeration phenomenon led to a reduction in the continuity of protective surface oxide layers, rendering the Al-B<sub>4</sub>C composite more vulnerable to chloride ions and yielding a less noble electrochemical potential. Consequently, an escalation in the B<sub>4</sub>C content correlated with an increased corrosion rate. Notably, the Brinell hardness test results demonstrated that macrohardness exhibited improvement in tandem with the increasing presence of reinforced B<sub>4</sub>C particulates.

#### ACKNOWLEDGEMENTS

The author wishes to extend gratitude to the Malaysia Public Services Department (JPA) for their generous support through the HLP-JPA student scholarship, which facilitated the author's research endeavors. The authors also would like to thank the Ministry of Education Malaysia for the financial support through research grant FRGS/1/2020/TK0/UKM/02/35. Furthermore, the authors express their sincere appreciation to the Faculty of Science and Technology at Universiti Kebangsaan Malaysia for their invaluable guidance, technical expertise, and administrative assistance throughout the research process. Additionally, the authors extend their heartfelt

thanks to the Malaysian Nuclear Agency for their provision of essential facilities, equipment, and technical support, which were instrumental in enabling the successful execution of this work.

## REFERENCES

- [1] T. Dursun and C. Soutis, "Recent developments in advanced aircraft aluminium alloys," *Materials & Design (1980-2015)*, vol. 56, pp. 862-871, 2014/04/01/ 2014.
- [2] C. G. E. Mangin, J. A. Isaacs, and J. P. Clark, "MMCs for automotive engine applications," *JOM*, vol. 48, no. 2, pp. 49-51, 1996/02/01 1996.
- [3] S. Manu, N. Radhika, V. Sidvilash, and T. J. T. i. I. Mohanraj, "Investigation on the mechanical and wear behaviour of Al-6082-BN-B4C-corn cob ash hybrid composites," vol. 44, no. 2, p. 294, 2022.
- [4] K. Suganeswaran, R. Parameshwaran, T. Mohanraj, and N. Radhika, "Influence of secondary phase particles Al<sub>2</sub>O<sub>3</sub>/SiC on the microstructure and tribological characteristics of AA7075-based surface hybrid composites tailored using friction stir processing," vol. 235, no. 1, pp. 161-178, 2021.
- [5] E. A. ASSOCIATION, *GOLDMAN SACHS GLOBAL INVESTMENT RESEARCH*, 20 JUNE 2021.
- [6] M. K. Kulekci, "Magnesium and its alloys applications in automotive industry," *The International Journal of Advanced Manufacturing Technology*, vol. 39, no. 9, pp. 851-865, 2008/11/01 2008.
- [7] R. Jolith, N. Radhika, and M. Govindaraju, "Reciprocating Wear Behavioural Analysis of Heat-treated Aluminium ZrO<sub>2</sub>/Al<sub>7</sub>Si<sub>0.3</sub>Mg Functionally Graded Composite Through Taguchi's Optimization Method," *Silicon*, vol. 14, no. 17, pp. 11337-11354, 2022/11/01 2022.
- [8] A. Handbook, *Properties and Selection: Irons, Steels, and High-Performance Alloys*. ASM International, 1990, p. 1063.
- [9] R. Mohanty, K. Balasubramanian, and S. K. Seshadri, "Boron carbide-reinforced aluminium 1100 matrix composites: Fabrication and properties," *Materials Science and Engineering A-structural Materials Properties Microstructure and Processing - MATER SCI ENG A-STRUCT MATER*, vol. 498, pp. 42-52, 12/01 2008.
- [10] F. Thévenot, "Boron carbide—A comprehensive review," *Journal of the European Ceramic Society*, vol. 6, no. 4, pp. 205-225, 1990/01/01/ 1990.
- [11] J. Abenojar, F. Velasco, and M. A. Martínez, "Optimization of processing parameters for the Al+10% B<sub>4</sub>C system obtained by mechanical alloying," *Journal of Materials Processing Technology*, vol. 184, no. 1, pp. 441-446, 2007/04/12/ 2007.
- [12] I. Aziz, Z. Qi, and X. Min, "Corrosion Inhibition of SiCp/5A06 Aluminum Metal Matrix Composite by Cerium Conversion Treatment," *Chinese Journal of Aeronautics*, vol. 22, no. 6, pp. 670-676, 2009/12/01/ 2009.
- [13] I. B. Singh, D. P. Mandal, M. Singh, and S. Das, "Influence of SiC particles addition on the corrosion behavior of 2014 Al-Cu alloy in 3.5% NaCl solution," *Corrosion Science*, vol. 51, no. 2, pp. 234-241, 2009/02/01/ 2009.
- [14] M. S. N. Bhat, M. K. Surappa, and H. V. S. Nayak, "Corrosion behaviour of silicon carbide particle reinforced 6061/Al alloy composites," *Journal of Materials Science*, vol. 26, no. 18, pp. 4991-4996, 1991/09/01 1991.
- [15] V. A. Katkar, G. Gunasekaran, A. G. Rao, and P. M. Koli, "Effect of the reinforced boron carbide particulate content of AA6061 alloy on formation of the passive film in seawater," *Corrosion Science*, vol. 53, no. 9, pp. 2700-2712, 2011/09/01/ 2011.
- [16] Y. Li, Q.-l. Li, D. Li, W. Liu, and G.-g. Shu, "Fabrication and characterization of stir casting AA6061—31%B<sub>4</sub>C composite," *Transactions of Nonferrous Metals Society of China*, vol. 26, no. 9, pp. 2304-2312, 2016/09/01/ 2016.
- [17] K. Shirvanimoghaddam et al., "Boron carbide reinforced aluminium matrix composite: Physical, mechanical characterization and mathematical modelling," *Materials Science and Engineering: A*, vol. 658, pp. 135-149, 2016/03/21/ 2016.

- [18] A. Rao, M. Mohape, V. Katkar, D. Gowtam, V. Deshmukh, and A. Shah, "Fabrication and Characterization of Aluminum (6061)-Boron-Carbide Functionally Gradient Material," *Materials and Manufacturing Processes*, vol. 25, pp. 572-576, 07/01 2010.
- [19] T. J. A. Doel and P. Bowen, "Tensile properties of particulate-reinforced metal matrix composites," *Composites Part A: Applied Science and Manufacturing*, vol. 27, no. 8, pp. 655-665, 1996/01/01/ 1996.
- [20] Y. Han, D. Gallant, and X.-G. Chen, "Investigation on Corrosion Behavior of the Al-B4C Metal Matrix Composite in a Mildly Oxidizing Aqueous Environment," *Corrosion*, vol. 67, no. 11, pp. 115005-115005-11, 2011.
- [21] C. S. Ramesh, R. Keshavamurthy, B. H. Channabasappa, and A. Ahmed, "Microstructure and mechanical properties of Ni-P coated Si<sub>3</sub>N<sub>4</sub> reinforced Al6061 composites," *Materials Science and Engineering: A*, vol. 502, no. 1, pp. 99-106, 2009/02/25/ 2009.
- [22] A. Baradeswaran and A. Elaya Perumal, "Study on mechanical and wear properties of Al 7075/Al<sub>2</sub>O<sub>3</sub>/graphite hybrid composites," *Composites Part B: Engineering*, vol. 56, pp. 464-471, 2014/01/01/ 2014.
- [23] K. Kalaiselvan, N. Murugan, and S. Parameswaran, "Production and characterization of AA6061-B4C stir cast composite," *Materials & Design*, vol. 32, no. 7, pp. 4004-4009, 2011/08/01/ 2011.
- [24] M. Sambathkumar, R. Gukendran, T. Mohanraj, D. K. Karupannasamy, N. Natarajan, and D. S. Christopher, "A Systematic Review on the Mechanical, Tribological, and Corrosion Properties of Al 7075 Metal Matrix Composites Fabricated through Stir Casting Process," *Advances in Materials Science and Engineering*, vol. 2023, p. 5442809, 2023/01/21 2023.